RSC Advances

ROYAL SOCIETY OF CHEMISTRY

www.rsc.org/advances

ARTICLE

Defluoridation by rice spike-like Akaganeite anchored graphene oxide

Yuyang Iiu, [a] Jiaxin Lv, [a] Wei Jin[b]* and Yaping Zhao[a]*

Received 00th January 20xx,
Accepted 00th January 20xx

DOI: 10.1039/x0xx00000x

www.rsc.org/

Due to intake of excessive fluoride in drinking water, endemic fluorosis, the most widely distributed endemic diseases has caused worldwide attention. In this study, Akaganeite anchored graphene oxide (β-FeOOH@GO) nanocomposites were synthesized by in-situ forced hydrolysis of ferric chloride in presence of graphene oxide under facile condition. β-FeOOH@GO was characterized and evaluated as a new potential carbon sorbent for defluoridation in environmental application. The application pH, adsorption capacity, adsorption kinetic and anti-interference ability in defluoridation with β-FeOOH@GO was described. On the basis of Fourier Transform Infrared Spectroscopy (FTIR) and X-ray Photoelectron Spectroscopy (XPS) analysis, defluoridation mechanism involving the ion-exchange with chloride anions bearing in β-FeOOH@GO is indicated at molecular level from a new perspective way. It is a good supplement to classical hydroxyl replacement mechanism. It would be useful for the improvement of adsorption capacity and kinetics through designing facile anions-exchange adsorbents.

INTRODUCTION

Endemic fluorosis widely distributed among more than 40 countries and regions, such as India, Germany, Italian and China. Endemic fluorosis is caused by the long-term intake of excessive fluoride through the way of drinking water and inhalation of fluoride air/dust. High fluoride contaminated groundwater sources have become an important health-related geo-environmental issue in certain regions.[1, 2] More than 200 million people around the world intake excessive amounts of fluoride, of which about 80 million people in China. Endemic fluorosis is prevalence in 44 % of counties in China with fluoride concentration as high as 17 mg L^{-1} in some area in Heilongjiang Province. China has become the world's severely affected country by fluorosis poison in drinking water.[3, 4] Fluoride present in surface water is associated with anthropogenic resource, such as mineral and chemical process, and the natural dissolution of fluoride-bearing minerals or geochemical deposits. Fluoride concentration in groundwater is generally 1.0 ~ 3.0 mg L^{-1}, 2.85 mg L^{-1} is the threshold of causing dental and skeletal fluorosis (Turner et al., 2005). The World Health Organization (WHO) recommends that the concentration of fluoride in drinking water should be less than 1.5 mg L^{-1}.[5] "Drinking water health standard" of China GB5749-85 issued stringent fluoride regulation of 1.0 mg L^{-1}. A great number of methods of defluoridation from groundwater, such as coagulation-sedimentation by inorganic aluminum coagulants, membrane process, and adsorption, have been reported and studied in detail.[6] But so far no effective methods can be carried out successfully and routinely in any of those countries.

Among aforementioned methods, adsorption is one of the most popular and widely used methods of defluoridation. The desirable characteristics of adsorbent depend on the factors such as pH,

[a] School of ecological and environmental science, East China Normal University, Shanghai, 200241, China
[b] School of environmental science and Engineering, Tongji University, Shanghai, 200071 China

adsorption capacity in the presence of competing ions, stability, ease of operation, potential for reuse and economics in community and domestic level. The effectiveness of an adsorbent greatly depends on the physicochemical properties of the materials. Activated alumina is the most extensively studied adsorbent for removal of fluoride from drinking water for its acceptable capacity and relatively low operation cost. The performance of activated alumina is considerably limited by the pH requirement, hardness, irregularly and fine particles and secondary pollution of leaking toxic aluminum ions.[7, 8] A viable substitute for activated alumina, iron oxide, such as such as iron corrosion products, maghemite, magnetite, hematite or ferric oxyhydroxide (FeOOH) has been proved to be an effective alternative for defluoridation thanks to natural abundance, unique adsorption capacity, high reactivity. However, iron (oxy)hydroxide is usually present as fine or ultrafine particles, easy to agglomerate, to decrease the adsorption activity and difficult to be separated from water phase for its nano-size effect.[9, 10] Micro/nano-scale iron-based adsorbents have demonstrated preferable fluoride removal due to combine the specific fluoride uptake by iron oxide with the satisfactory hydraulic hydrodynamic properties of the carriers, and their applicability is much better than the bare iron oxide or sole carriers. Certain carriers, such as activated alumina, polymeric exchangers, activated carbon and silica would facilitate iron (oxy)hydroxide to disperse and reclamation.[3] For example, nanosized hydrous zirconium oxide within a commercial porous polystyrene anion exchanger D201which is a macroporous strongly basic anion exchanger of polystyrene matrix and chloride type. It exhibits enhanced fluoride removal as well as the satisfactory hydraulic properties for practical application.[11] The aluminum-impregnated carbon also shows several times enhanced adsorption capacity of fluoride than activated carbon.[12] Impregnation of metal oxide nanoparticles on matrix of materials, especially on three-dimensional porous resin would result in pores or channels blockage and possibly decrease the accessible adsorption sites.[13] Therefore, the novel nano iron (oxy)hydroxide carriers with high specific surface area and chemical stability are in demand for defluoridation. Within these several years, graphene based materials is widely used as carrier in environment. Graphene has the unique chemical structure of two dimensional, single layer of sp^2-hybridized carbon atoms, which determines its large specific surface area as highly as 2630 m^2 g^{-1}, light, chemical stability and nontoxic. Currently graphene based nano metal (oxy)hydroxide hybrid composites have greatly exhibited promising catalytic performances in semiconductors, electrochemical performances of energy-storage/conversation in fuel cells, supercapacitor and environmental application.[14] As far as defluoridationn in water, only aluminum and manganese oxide/salt coated graphene were reported until now, i.e. defluoridation by basic aluminum sulfate@graphene hydrogel, Graphene oxide–aluminum oxyhydroxide and manganese oxide coated graphene oxide.[15, 16] Hence it can be confirmed that suitable incorporation metal oxide with graphene oxide would significantly improve the adsorption capacity of anion pollutants in relation to its precursor graphene oxide. Ca, Zr, La, Al, Mn and Fe oxides are the most studied metal (oxy)hydroxides due to high reactivity

towards anions.[17-22] It would be the best way to promote its environmental application when given full paly of synergic function of iron (oxy)hydroxide with graphene as novel potential fluoride adsorbent.

In order to better understand ion-exchange mechanism, a new insight on predominate mechanism of fluoride uptake is elucidated through exchanging with chloride coprecipitated in β-FeOOH@GO in this study. It would be a good supplement to the classical ion exchange mechanism of replacement of hydroxyl groups occurring in metal oxide structure. A series of experiments under a function of solution pH, kinetics, thermodynamics, competing anions, adsorption-regeneration were carried out to explore the performance and feasibility of β-FeOOH@GO for application of defluoridation. The aim of clarifying the adsorption mechanism may contribute to design efficient anions-bearing adsorbent for optimizing the environmental application.

Materials and methods

Chemicals and materials

Graphite was purchased from Institute of Guangfu Chemical (Tianjin, China). Sodium fluoride (NaF), ferric chloride hexahydrate ($FeCl_3$•$6H_2O$), potassium permanganate (KMnO4), hydrogen peroxide (H_2O_2, 30 %), concentrated sulfuric acid (H_2SO_4, 98 %) and all other chemicals were analytical reagent grade and purchased from Sinopharm Chemical Reagent Co. Ltd (Shanghai, China). All the chemicals were used as received without further purification. Stock solution of 1000 mg L^{-1} fluoride was prepared by dissolving 2.21 g of NaF in 1 L deionized water and stored in polyethylene bottle at 0 ℃. Deionized water was used throughout the experiments.

Synthesis and characterization of β-FeOOH@GO

Graphene oxide (GO) was prepared from natural graphite powder using modified Hummer's methods.[23] Briefly 2 g of graphite powder was added to ice water cooled concentration H_2SO_4 (100 ml). Then, 12 g of $KMnO_4$ were added gradually while stirring. The mixture was then transferred to a 30 ℃ water bath and stirred for 60 min. 250 ml deionized water was slowly added and the temperature increased to 98 ℃ and maintained for 30 min. When the temperature was reduced to 60 ℃, 20ml of H_2O_2 (30 %) was dropped into the suspension to completely react with the excess $KMnO_4$ and produced a bright yellow mixture indicating the oxidation of pristine graphite to GO. Then, the mixture was filtered and washed with diluted HCl to remove metal ions. Finally, the product was washed repeatedly with deionized water until the pH was neutral. The sample of GO was dried at 60 °C and stored.

β-FeOOH@GO nanocomposite was synthesized following the method of in-situ hydrolysis in presence of GO and $FeCl_3$. 0.1 g of GO was mixed with 100 ml volume of water in conical flask and sonication for 30 min. Then 2.7 g of $FeCl_3$•$6H_2O$ was added into above mixture with magnetic stirring to form a homogeneous solution. Subsequently, the mixture was stirred in the water bath at 80 °C for 4 h. The resulting precipitate was separated by centrifugation and washed with water and absolute ethanol to remove impurities. The

sample was dried in an oven at 60 °C until it was completely dried. The sample was then manual powdered and stored in an air-tight container.

The crystalline phase of β-FeOOH@GO was characterized by X-ray diffraction (XRD, Rigaku D/Max-2500, Japan) employing Cu Kα as source of radiation, λ = 1.54056 Å at a scan speed of 10 ° min^{-1} over an angular range between 5 ° to 70 °. The morphology and size of the samples were characterized by using a field emission scanning electron microscope (SEM, S-4800, Hitachi, Japan) and transmission electron microscopy (TEM, HT7700, Hitachi, Japan) operating voltage of 200 kV. The Fourier transform infrared (FT-IR) spectrum was recorded with a GX spectrophotometer (Perkin Elmer, USA) with the KBr wafer technique. The surface analysis of adsorbents using X-ray photoelectron spectroscopy (XPS) were acquired with an Axis UltraDLD spectrometer (Kratos Analytical-A Shimadzu group company, Japan) using a monochromatic Al Kα source (1486.6 eV). The binding energies were referenced to the C1s peak at 284.6 eV and fitted by XPSPEAK41 program with a Shirley background subtraction and Gaussian−Lorentzian (20−30 %) as fitting functions.

Batch adsorption experiments

The fluoride adsorption tests were performed using the completely mixed batch reactor techniques. The effects of pH were carried with 0.05 g of adsorbents separately equilibrated in a serial of 100 ml conical flasks containing 20 ml of 25 mg L^{-1} fluoride solution. The pH was adjusted to desired values with 0.1 M HNO_3 or 0.1 M NaOH solutions. The solutions were agitated at 160 rpm and at 25 ℃ in a water bath thermometer over 8 h. The content was withdrawn at various time intervals and filtered with 0.45 μm membrane to analyze the residual fluoride concentration using fluorine reagents spectrophotometry (UV1120, Tianmei science technology Ltd in Shanghai, China). The equilibrium adsorption capacity (in milligrams per mass unit of adsorbent) and removal rate were calculated on the basis of mass balance. The total soluble iron content was determined by inductively coupled plasma-atomic emission spectrometry (ICP-OES optimal 8000, Perkin Elmer, USA) and proper calibration was also performed to ensure the consistency of the different methods and detection limit is 0.03 mg L^{-1}.

The adsorption kinetics was carried out as following: 500 mg of adsorbents was separately equilibrated in a serial of conical flasks containing 300 ml of 25 mg L^{-1} fluoride solution without adjusting their pHs. The contents were agitated in 160 rpm at 25, 35 and 45 ℃ in a water bath thermostatic oscillator, respectively. The adsorption isotherms were tested as that of pH experiments except at varying initial fluoride concentrations of 10，25, 50, 75, 100, 150,200 and 250 mg L^{-1}. The influence of coexisting anions on fluoride adsorptions were carried as that of pH experiments except in presence of desired concentration of common ions (i.e. 250 mg L^{-1} of SO_4^{2-}, Cl-, NO_3^- and HCO_3^-, respectively, 25 mg L^{-1} of SiO_3^{2-} and PO_4^{3-}). In the adsorption-desorption recycle experiment, 1 mol L^{-1} NaOH or HCl were used to regenerate the fluoride saturated adsorbents. Other procedures were performed according to aforementioned.

Results and discussions

Characterization of β-FeOOH@GO

Due to its tunnel structure nano-sized Iron (oxy)hydroxide (FeOOH) has been found application in the field of catalyst and adsorbent to remove toxic elements polluted environment. The chemical, structural and physical properties of FeOOH, such as crystalline, morphology and particle size, are mainly determined by the composition of iron salt and initial hydrolysis pH of preparation conditions applied. Akaganéite anchoring on the graphene oxide (β-FeOOH@GO) nanocomposite was prepared through a simplest and moderate way by in-situ hydrolysis of $FeCl_3$. The as-prepared β-FeOOH@GO and GO were characterized by XRD shown in Fig. 1. The sharp and narrow peak at 2θ=10.6 ° can be assigned to crystal characteristic diffraction peak d_{001} of GO with the interlayer spacing of 0.834 nm according to Bragg Equation. The interlayer spacing of GO is larger than 0.34 nm of natural graphite. The increased interplanar spacing results from the presence of abundant oxygen containing functional groups causing a highly hydrophilic propriety. The XRD pattern of β-FeOOH@GO can be well indexed to the diffraction peaks of akaganéite-M, syn (JCPDF card No. 34-1266). The very sharp peaks indicate high crystallinity of synthesized β-FeOOH. The diffraction peaks of GO are totally vanished, it could be deduced that the regular stack of GO was destroyed by the intercalation of β-FeOOH nanoparticles.

The surface texture and morphology of β-FeOOH@rGO were observed using SEM and TEM. In Fig. 2a and 2b, the morphology of manual powdered β-FeOOH@GO was basically the rice-spike like nanorod with the length of 50-150 nm compacting on GO. From low magnification TEM images in Fig. 2c and 2d, it can be clearly found that the cross section of rice-spike like β-FeOOH nanorod was with the dimensions of about 100 nm of length × about 20 nm of width attached on the wrinkled transparent surface of layered GO sheet. Based on the High resolution TEM characterization in Fig. 2e to 2f, the morphology of rice-spike like Polydomainic nanorod crystal is inferred to be smaller nanoparticle aggregates. De Bruyn et al. explained the hydrolysis mechanism of Fe(III) salt by inferring a three-step hydrolysis process consisting of formation of the polymer spheres-like nanoparticles from low-molecular-weight species, aggregation and subsequent precipitation.[24-27] Simultaneously the oxygen-containing functional groups of GO joining the formation of octahedral β-FeOOH as chelating groups, further facilitated the tightly fixation of β-FeOOH particles on GO sheet.[24, 25] TEM images of β-FeOOH@GO indicates β-FeOOH uniformly anchored on the GO sheet, which would be expect to display large accessible surface area and reaction activity than that of β-FeOOH aggregates. The structure of β-FeOOH@GO would greatly influence its environmental adsorption and separation function.

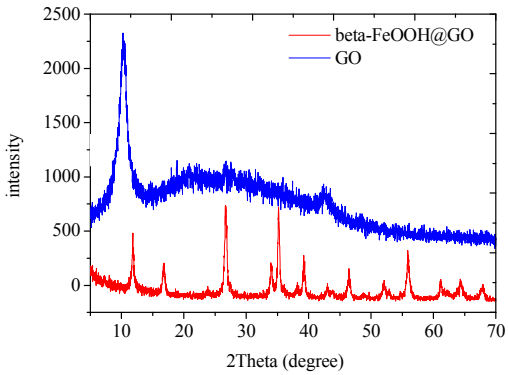

Fig. 1 X-ray diffraction patterns of GO and β-FeOOH@GO.

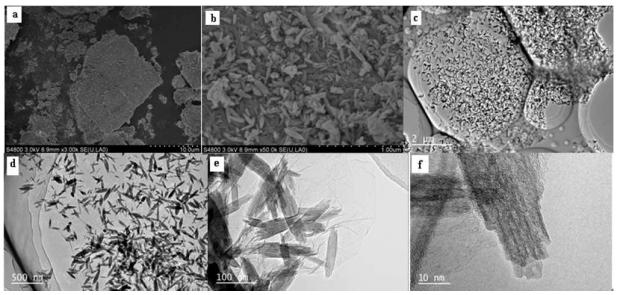

Fig. 2 SEM images of β-FeOOH@GO (a and b) and TEM images of β-FeOOH@GO(c to f).

Effect of pH

pH is one of important variables that affect fluoride removal from interface of water and solid adsorbents. The adsorption of fluoride by β-FeOOH@GO and desorption of chloride from β-FeOOH@GO were evaluated at different pH values and results shown in Fig. 3. The adsorption capacity of β-FeOOH@GO towards fluoride showed a similar uptake rate when pH values ranged from 2.1 to 10.4, with the maximum adsorption rate around 80 %. The adsorption of fluoride results in an obviously drop from pH 11.1 to 12.7, even dropping from 45.8 % to 17.6 %. Chloride desorption evolvement from β-FeOOH@GO was monitored within this pH range. The maximum desorption of chloride was around 54 mg L^{-1} from pH 2.1 to 10.4, then obviously increased from 65.3 to 88.3 mg L^{-1} with increase pH 11.1 to 12.7. This phenomenon indicated the anion exchange nature. No detectable leached iron was observed in the whole pH range, indicating the stability of the adsorbent. The pH_{ZPC} of β-FeOOH is about 8.0-8.5. When pH increased near 8.0, the fluoride anions speciation (pKa of 3.18) predominantly exists in the solution. According to surface potential theory, positively charged β-FeOOH would be favourable to interact with fluoride through electrostatic force. When pH increased to more than 10.5, there would has competition between the gradually increased negative surface charge of β-FeOOH and fluoride to slightly hinder the fluoride adsorption by electric repulsion but never eliminate the fluoride removal. Gradually increased pH would drive the defluoridation reaction to occur because the adsorbed the fluoride can be easily desorbed with 0.1 mol L^{-1} NaOH.[28] Fluoride adsorption is strong dependent on surface charge of β-FeOOH not that of GO because GO interacts with fluoride only through a nonspecific ion exchange or Columbic interaction. The electrostatic adsorption was probably not the only mechanism to remove fluoride within whole pH range. Just as Tang and co-authors reported that the fluoride adsorption on ferrihydrite surface was a combination of both anion exchange and van der Waals forces.[29] Mixed nano iron oxides powder containing goethite (alpha-FeOOH), hematite (alpha-Fe_2O_3) and ferrihydrite ($Fe_5HO_8{\cdot}4H_2O$) was synthesized and tested its fluoride adsorption capacity. By varying the initial pH in the range of 3.0–10.0, maximum adsorption was observed at a pH of 5.7.[30] Chen and co-authors shows the fluoride adsorption capacity of BAS@GHG-2 increases with pH from pH 3.8 to reach a maximum value of 35 mg g^{-1} at pH 7.2 and decreases until pH 11.8. The optimum pH range for BAS@GHG-2 adsorbent is 7–8.[15] Pan and co-authors reported that HZO-201 had the highest capacity for fluoride uptake at pH 3.0, and then decrease of pH to 2.0 or increase to 9.0 would obviously decrease the adsorption rate, and at pH 9.0 the capacity even approached to zero. [11] Comparing

with those researches, β-FeOOH@GO shows a relatively wide application of pH range due to its chemical adsorption nature with fluoride.

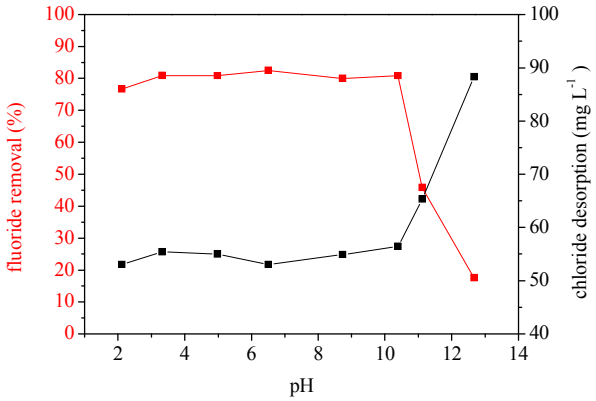

Fig. 3 Effect of pH on fluoride removal and chloride desorption by β-FeOOH@GO.

Adsorption kinetics

The adsorption kinetics of fluoride at various temperatures was graphically illustrated in Fig. 4. It is clear to see that the adsorption increases with the temperature, indicating the process is endothermic in nature. The majority adsorption reaches equilibrium within 60 min and shows fairly fast kinetic rates. With the accumulation of fluoride on the surface, the adsorption rate slows down until equilibrium. The equilibrium is independent of temperature. For statistical analysis fluoride adsorption kinetics and potential rate-controlling steps, the experiments data were fitted by nonlinear regression to the pseudo-first-order kinetic, second-order kinetic and Weber–Morris models: [31, 32]

Pseudo-first-order kinetic model equation:

$$\frac{dq_t}{dt} = k_1(q_e - q_t) \quad (1)$$

It can be integrated to:

$$\ln(q_e - q_t) = \ln q_e - k_1 t \quad (2)$$

$$q_t = q_e(1 - e^{-kt}) \quad (3)$$

Pseudo-second-order kinetic model equation:

$$\frac{dq_t}{dt} = k_2(q_e - q_t)^2 \quad (4)$$

It can be integrated to:

$$q_t = q_e \times \frac{q_e \cdot k_2 \cdot t}{1 + q_e \cdot k_2 \cdot t} \quad (5)$$

Weber–Morris model equation:

$$q_t = k_p\ t^{1/2} \quad (6)$$

In which q_t and q_e are adsorption capacity at any time and at equilibrium (mg g^{-1}), respectively. k_1 and k_2 are Pseudo-first-order or second-order reaction rate constants, respectively. k_p (mg g^{-1} min^{-1}) is the intraparticle diffusion constant and t is time. To understand the dynamics of fluoride adsorption, the kinetic data fitting results of Pseudo-first or second order kinetic model were shown in Fig. 4 and Table 1. The fitting results are close to the experimental measurements with high R^2. Pseudo-second model can better describe the gradual adsorption process until equilibrium which implied the adsorption mechanism would be chemisorption process. The calculated equilibrium adsorption capacity 14.59 mg g^{-1} is consistent with the experimental value of 14.94 mg g^{-1}. Therefore increasing the temperature shift the adsorption equilibrium to the right, the kinetic rate

constant increases accordingly producing the apparent activation energy of 29.77 kJ mol^{-1} by fitting with the linear Arrhenius equation:

$$\ln k = \ln A - Ea/(RT) \quad (7)$$

Where A is the pre-exponential factor, Ea the apparent activation energy and R the gas constant.

The three consecutive steps in the adsorption of adsorbates by a porous adsorbent are: 1) transport to the external surface of the adsorbents. At this moment, the adsorbent has a lot of active adsorption sites on its surface, combing with the mass transfer driving force caused by High concentration difference of fluoride, showing relative rapid fluoride adsorption reaction, which was usually interpreted as an external diffuse process (film diffuse); 2) transport to the pores of the adsorbents. At this stage, usually, diffusion of the adsorbates into the adsorbent pores occurs (particle diffusion); 3) exterior surface chemical adsorption (chemical reaction). According to Weber–Morris equation, the intraparticle diffusion as the rate-limiting step is fairly clear. It shows that a distinct fast diffusion pathway controlling the initial adsorption kinetics followed by relatively slow diffusion prior to adsorption equilibrium. It may be ascribed to GO inhibit the aggregation of nano-sized β-FeOOH which in return to provide more accessible surface areas for fluoride.

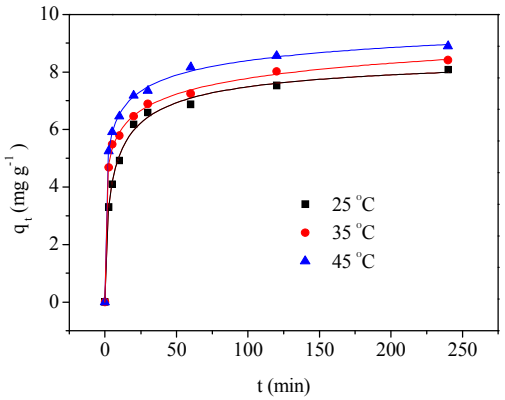

Fig. 4 Adsorption kinetic plots of fluoride adsorption on β-FeOOH@GO.

ARTICLE

Table 1 Kinetic parameters for adsorption of fluoride by β-FeOOH@GO

T	Pseudo-first order			Pseudo-second order			Experimental
(℃)	k_1 (min^{-1})	q_e (mg g^{-1})	R^2	k_2 (g mg^{-1} min^{-1})	q_e (mg g^{-1})	R^2	q_e (mg g^{-1})
25	0.1587	7.0991	0.9259	0.0290	7.7167	0.9811	8.084
35	0.3213	7.2197	0.8956	0.0600	7.7392	0.9598	8.412
45	0.3392	7.8292	0.9119	0.0613	8.3487	0.9700	8.900

	Weber–Morris	
T (℃)	K_p	R^2
25	0.1211	0.995
35	0.1186	0.998
45	0.1097	0.998

Adsorption isotherms

The effect of temperature on the adsorption isotherm of fluoride and desorption of chloride were tested with variable initial fluoride concentrations and result was shown in Fig. 5. At a certain temperature, the adsorption capacity was increased with fluoride initial concentration. A slight enhancement in the adsorption capacity for fluoride as a function of temperature was also observed indicating an endothermic process. Accordingly, desorption of chloride increased from 48.6 to 58.3 until equilibrium around 60 mg L^{-1} with fluoride concentrations at 25 ℃. It proved ion exchange nature during the adsorption of fluoride. The fluoride adsorption results were usually used Langmuir and Freundlich isotherm models to describe：[33, 34]

Langmuir isotherm: $$q_e = \frac{bq_m C_e}{1 + bC_e} \quad (8)$$

Freundlich isotherm: $$q_e = kC_e^{\frac{1}{n}} \quad (9)$$

Where c_e and q_e are equilibrium concentration of fluoride and equilibrium amount of fluoride adsorbed by adsorbent. Where b and qm are Langmuir constant and the maximum adsorption capacity of fluoride adsorbed by the adsorbent. Where Freundlich constant k and 1/n are the minimum sorption capacity of fluoride adsorbed by the adsorbent and adsorption intensity. The Langmuir and Freundlich models fitting results were shown in Table 2. A higher value of the Freundlich adsorption coefficient (k) indicates a higher affinity of adsorbent-adsorbate. The constant values of n in the range of 2–10, 1–2 and <1 associated with good, moderate poor and poor adsorption characteristics, respectively. Comparing with the corelation coefficient, Freundlich isotherm models can provide a more satisfactory fitting quality. The constant n is higher than 2 indicating the adsorption is favoured in current study. The Langmuir adsorption model gave a maximum adsorption capacity of fluoride on the adsorbent was about 23.58 mg g^{-1} at 25 ℃ in relation to the lower adsorption ability of GO of 1.6925 mg g^{-1} under the conditions tested in this study due to the non-electrostatic interaction. β-FeOOH@rGO also exhibited a pronounced advantage than that of classical adsorbent, such as Activated Alumina of 1.08 mg g^{-1}, polymeric resin of 3.62 mg g^{-1} and activated carbon of 0.075 mg g^{-1}, respectively.[33, 34] It also can be compared with current reported results of manganese oxide coated graphene oxide with an adsorption capacity of 11.93 mg g^{-1}, Basic aluminumsulfate@graphene hydrogel possessing an adsorption capacity of 33.40 mg g^{-1} and aluminum oxyhydroxide modified graphene oxide showing an adsorption capacity of 51.42 mg g^{-1}, separately.[15, 16, 35] Just like preparation method, starting metal salt, surface area, crystalline structure and so on, the type of metal oxide is still an important factor influencing the adsorption capacity of fluoride.

Thermodynamic parameters were calculated to assess the thermodynamic spontaneity and feasibility of the adsorption process, such as changes in Gibbs free energy (ΔG_0), enthalpy(ΔH_0), and entropy(ΔS_0) (shown in Table 2). Equations are as follows:

$$\Delta G_0 = -RTIn(K_0) \quad (10)$$

$$\Delta G_0 = \Delta H_0 - T\Delta S_0 \quad (11)$$

Where T (K) is the temperature, R (8.314×10-3 kJ.mol K) is the universal gas constant and K_0 is the thermodynamic equilibrium constant. The thermodynamic equilibrium constant (K_0) for the process is determined by plotting $ln(q_e/c_e)$ versus q_e, and extrapolating to zero qe using a graphical method fitted through the data points by the least squares method. The intersection with the vertical axis gives the value of K_0. Values of ΔS_0 and ΔH_0 are evaluated from the slope and intersect of plotting ΔG_0 versus T. The calculated ΔG_0 value indicated that the fluoride adsorption by β-FeOOH@rGO was spontaneous and was favouring of adsorption process by temperature. The positive value of ΔH_0 indicates the endothermic nature of the sorption. The values of ΔS_0 showed the disorder enhancement on the solid liquid interface.[36]

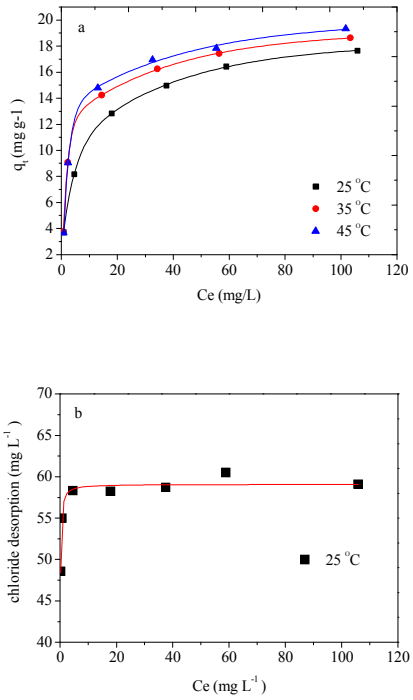

Fig. 5 Adsorption isotherm (a) and chloride desorption plots (b) of fluoride on β-FeOOH@GO

Effect of common anions and cycles of reuse

The co-existing anions in water matrix will compete with fluoride for the adsorption active sites. The effect of co-existing anions on the adsorption of fluoride was shown in Fig. 6. In general, their effect on defluoridation was in the sequence of HCO_3^- > SO_4^{2-} > PO_4^{3-} > SiO_3^{2-} > NO_3^- > Cl^-. Bicarbonate caused about 30 % reduction of fluoride adsorption capacity due to form inner-sphere surface complex of bicarbonate. Just as the presence of high bicarbonate in water resources will accelerate the release of fluoride from the minerals under favourable geophysical conditions, because of replacement role of bicarbonate.[37] Decreasing bicarbonate concentration may eliminate this negative effective of fluoride adsorption. The existence of high concentration of silicate and phosphate only cause less than 10 % reduction to the adsorption of fluoride. Fluoride adsorption capacity doesn't decrease substantially when presence of phosphate, silicate and sulfate. Adsorption mechanism of those coexisting anions occurs via weaker bonds of outer-sphere complexation with the available active sites, while SO_4^{2-} forms both outer-sphere and inner-sphere complexes with the active sites in aqueous systems.[38] Low affinity ligands of Cl^- and NO_3^- nearly don't influence fluoride adsorption capacity. This indicates that anions with lower ionic potentials tend to be less preferably adsorbed by adsorbent, and also reflects the relatively competitive and inhibitive effects of these anions on the fluoride adsorption.[9] Mohapatra et al. reported the same results as far as the sulfate and chloride influence.[30] In Fig. 3, the hydroxyl would have a strong competition with fluoride when pH is more than 12. It would be expected that the adsorbent can be reused by adopting suitable regeneration methods. The result of regeneration and recyclability of β-FeOOH@rGO after six consecutive adsorption–desorption cycles were shown in Fig. 7. The percentage of adsorption of fluoride by β-FeOOH@GO was reduced from 76 % to 26 % following six cycle of operation using HCl as regenerant. The NaOH shows poor regeneration ability over HCl to provide available sites on adsorbent surface. Comparable effects were observed by several other authors.[39] The results suggest that the prepared β-FeOOH@rGO adsorbent could be partly generated via NaOH and HCl treatment. The effective regenerants should be explored to expand the application of the

adsorbent, such as combining NaOH followed acid solutions.[39]

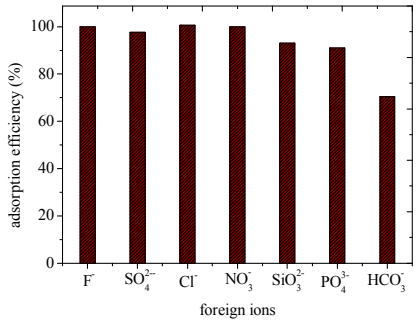

Fig. 6 Effect of foreign anions on fluoride adsorption on β-FeOOH@GO.

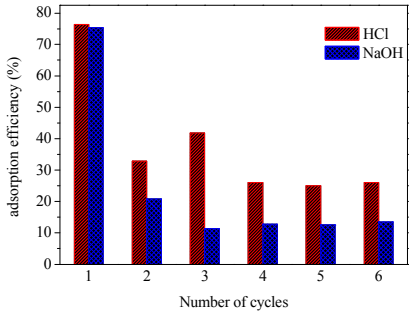

Fig. 7 The uptake of fluoride by β-FeOOH@rGO in different cycles of regeneration.

Table 2 Dynamic parameters for fluoride adsorption by β-FeOOH@GO

T	Langmuir			Freundlich			Thermodynamic parameters		
	b	q_{max}					ΔG_0	ΔH_0	ΔS_0
(℃)	(L mg^{-1})	(mg g^{-1})	R^2	k	n	R^2	(kJ mol^{-1})	(kJ mol^{-1})	(kJ mol^{-1} K)
25	0.1917	17.6722	0.963	5.5088	3.4670	0.960	-0.4475		298.4731
35	0.3992	18.0137	0.978	6.8907	4.3771	0.914	-1.8890	+48.322	307.2950
45	0.3293	19.0125	0.987	6.9057	4.2069	0.889	-3.7164		318.4786

Adsorption mechanism of fluoride

The loading of β-FeOOH on graphene oxide and adsorption of fluoride on β-FeOOH@GO were confirmed by FTIR in Fig. 8. The characteristic peak of GO at 3355 cm^{-1} is attributed to the O-H stretching vibration of adsorbed water molecule and GO structural OH groups. The characteristic peak at 1710 cm^{-1} and 1590 cm^{-1} can be due to the C=O and C=C groups, respectively. Peaks at 1028 and 1170 cm^{-1} were due to the deformation of C-O stretching vibration. The IR spectrum of β-FeOOH@GO were showing O-H peak weakening shift from 3338 cm^{-1} to 3303 cm^{-1}. The peaks of 3430-3100 cm^{-1}, 1610 cm^{-1} and 1060 cm^{-1} were assigned to the hydroxyl stretching vibration, H–O–H deformation vibration and the bending vibration of the surface hydroxyl group of β-FeOOH, respectively.[18] The peaks of 900–450 cm^{-1} belong to the characteristic peak of β-FeOOH. The intense characteristic peaks of β-FeOOH at 852 cm^{-1} and 665 cm^{-1} were assigned as characteristic Fe-O-H bending vibration and Fe-O or Fe-OH symmetric stretching or lattice vibration, separately. Mohapatra et al.[30] thought

those two peaks were ascribed to the vibrating modes of O-H-Cl hydrogen bonds, representative characteristics of Cl-containing akaganéite. After fluoride adsorption, the peak at 1060 cm^{-1} disappeared, peaks at 1610 and 665 cm^{-1} clearly weakened, and new peak at 919 cm^{-1} was attributed to the Fe and F interaction corroborating the exchange between Fe surface ligands with fluoride anions. This indicated that fluoride was bound through Fe-O bonding to form inner-sphere surface complex due to fluoride adsorption on the corresponding hydroxyl and/or anion ligands (Cl in this study) site. β-FeOOH@GO would be a good exchanger for monovalent anions, such as F^-, Cl^- and OH^-.

In the XPS wide scan spectrum shown in Fig. 9 and Table 3, the peaks located at 712.1, 531.3, and 284.6 eV are assigned to the characteristic peaks of Fe 2p, O 1s, and C 1s, respectively, which show the successful anchoring β-FeOOH on the surface of GO. The loading content of Fe is 25.7 % in mass. In the sample before fluoride adsorption Cl 2p peak was observed around 197.8 eV, indicating that chloride anions incorporated into β-FeOOH, thus the β-FeOOH crystal structure is iron (oxy)hydroxide containing chloride.[40] The chloride anions also have a great effect on the fast aggregation or aging of polymer spheres.[24, 25] The principal effect of Cl^- on aging of the polymer is that the final precipitated product is β-FeOOH nanorod which was to some extent crosslinked in presence of Cl^- anions.[41] FeOOH consists of double bands of edge-sharing $FeO_3(OH)_3$ octahedra linked by corner-sharing to form “tunnels”. Whereas the structure of β-FeOOH, contains squared molecular channels bounded by four double rows of $FeO_3(OH)_3$ octahedral and the channel is large enough to accommodate 1-9 wt% of Cl which appears to be essential for the structural stability.[41] Usually, fluoride is mostly based on replacing singly coordinated hydroxyl or water groups from the surface of FeOOH.[21] While other research thought the molecular channels of β-FeOOH are filled with water molecules and chloride anions belonging in the coordination shell of the Fe. Comparing with the sample after fluoride adsorption, Cl 2p peaks remarkably weakened (decreased about 48 %) and the F 1s peak locating at 684.2 eV obviously appeared. This phenomenon indicates chloride ions in β-FeOOH@GO may take part in the anion exchange with fluoride. It was also proved by our results of Fig. 3 and 5b. Compared with hydroxide anions, chloride has lower affinity for iron, therefore, in the thermodynamic sense, it is easier to replace chloride by fluoride rather than hydroxide anions. In Fig. 9b, the O 1s region could be deconvoluted into four overlapped peaks at 529.7 eV, 531.3 eV, 532.9 eV and 534.7 eV, corresponding to Fe-Ooxide and Fe-OH in lattice structure oxygen, Fe-OHads and H_2Oads in adsorbed oxygen. However, in Table 3, the content of H_2O is changed (19.9 % before adsorption and 17.8 % after adsorption of fluoride) suggesting the releasing of free H^+ to the solution from chelating H_2O from β-FeOOH@GO. The final pHs of equilibrated solution increased in the acid pH (pH < 4) and decreased in the circumneutral to alkaline pH range throughout this study. Due to the heterogeneity of the adsorption sites, each type of adsorption reaction mechanism may be complex. Based upon classical adsorption mechanism of exchanging of hydroxyl groups, the adsorption mechanism is

suggested. At low pH, hydroxyl group is protonated and facilitates the ligand exchange because the OH_2^+ is easier to be displaced by fluoride anions. The ion exchange is also occurring between the chloride anions within the tunnel of β-FeOOH with fluoride. The releasing of H^+ into the solution would occur from circumneutral to alkaline pH. The mechanism is shown in equation (12) and (13):

At low pH, mainly

≡Fe—OH(contained Cl) (solid)+H^+(aq)+F^-(aq) →

≡Fe—(OH_2^+…F^-)(contained F) (solid)+Cl^-(aq) →

≡Fe—F(contained F) (solid)+Cl^-(aq)+H_2O

(12)

From circumneutral to alkaline pH, mainly

≡Fe—OH_2 (contained Cl) (solid)+OH^-(aq)+F^-(aq) →

≡Fe—OH(contained F) (solid)+H_2O+Cl^-(aq)

(13)

Consequently, the adsorption capacity and kinetics of β-FeOOH is improved due to the existence of GO and chloride. This adsorption mechanism provides us with a new insight to the synthesis of metal oxide adsorbents with high content of the surface exchangeable anions to improve the performance of adsorption capacity.

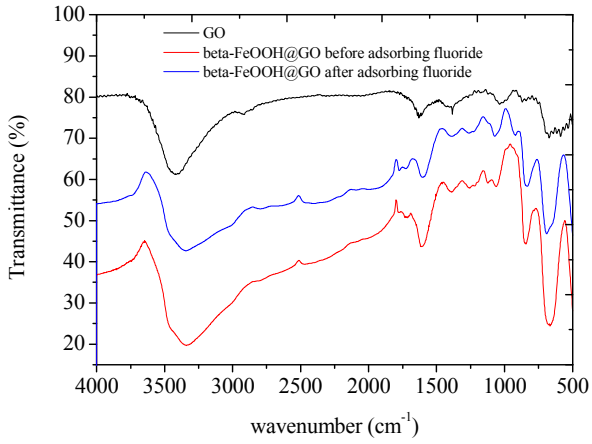

Fig. 8 FTIR spectra of GO, β-FeOOH@GO and fluoride adsorption on β-FeOOH@GO.

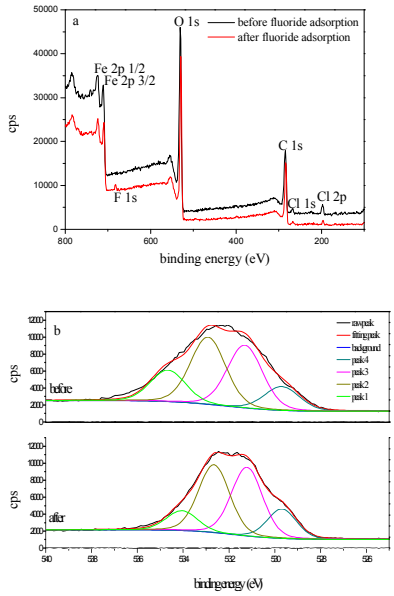

Fig. 9 Wide scan XPS spectra of β-FeOOH@GO before and after fluoride (a) and XPS spectra of O 1s deconvolution (b).

Table 3 Binding energy of and atomic surface concentration of β-FeOOH@GO

	Binding energy (eV)							
	Fe 2p		O 1s			F 1s	Cl 2p	C 1s
Before	712.1	529.8	531.1	532.4	533.3	no	197.8	284.6
after	711.6	529.7	531.1	532.3	533.2	684.2	197.8	284.8
	Atomic surface concentration (%)							
	Fe	O				F	Cl	C
		Fe-Ooxides	Fe-OH	Fe-OHads	H_2Oads			
Before	5.90		41.15			0	2.07	50.88
		13.8%	24.4%	28.2%	19.9%			
after	5.91		39.88			0.90	1.08	53.23
		15.6%	30.5%	26.3%	17.8%			

Conclusions

The akaganéite anchored graphene oxide (β-FeOOH@GO) was prepared in one-step hydrolysis method and characterized through XRD, SEM and TEM. The rice spike-like nanoparticles of β-FeOOH was observed uniformly dispersed on the GO sheet, which providing fluoride with large amount of accessing adsorption sites. With batch adsorption studies, fluoride adsorption process showed high kinetic to reach equilibrium within 60min and followed second-order kinetics, the maximum adsorption capacity of 17.67 mg g^{-1} at room temperature by fitting adsorption data to the Langmuir isotherm. Thermodynamic study revealed that adsorption process was spontaneous and endothermic in nature. Initial pH from 2.1 to 10.4 had little effect on fluoride adsorption. The adsorbent showed strong anti-interference ability for the presence of high concentration of common ions in water matrix. The FTIR and XPS results proved that the uptake of fluoride proceeding by an ion-exchange mechanism with chloride contained in β-FeOOH crystal structure. This work demonstrates the important role

of the surface chloride anions in fluoride removal, and also brings forward an important approach to the synthesis of metal oxide adsorbents with high content of the exchangeable anions, which should be of importance for both theoretical investigations and practical water treatment applications.

Acknowledgements

This research was financed by the National Natural Science Foundation of China (no. 21377039) and the Shanghai international cooperation research projects (no.14230710900).

References

1 S. Jagtap, M. K. Yenkie, N. Labhsetwar, S. Rayalu, *Chem. Rev.*, 2012, **112**, 2454.
2 M. T. Alarcón-Herrera, J. Bundschuh, B. Nath, H. B. Nicolli, M. Gutierrez, V. M. Reyes-Gomez, D. Nuñez, I. R. Martín-Dominguez, O. Sracek, *J. Hazard. Mater.,* 2013, **262**, 960.
3 A. Bhatnagar, E. Kumar, M. Sillanpää, *Chem. Eng. J.*, 2011, **171**, 811.
4 B. K. Handa, *Ground Wat.*, 1975, **13**, 275.
5 World Health Organization, *WHO*, Geneva, 2011.
6 V. J. Sachin, E. Bringas, G. D. Yadav, V. K. Rathod, Marathe Ortiz, K. V. Marathe, *J. Environ. Manage.*, 2015, **162**, 306-325.
7 F. J. Rubel, *J. Am. Water Works Assoc.*, 1979, **71**, 45.
8 S. Ghorai, K. K. Pant, *Chem. Eng. J.*, 2004, **98**, 165.
9 Y. H. Huang, Y. J. Shih, C. C. Chang, *J. Hazard. Mater*., 2011, **186**, 1355.
10 L. H. Velazquez-Jimenez, E. Vences-Alvarez, J. L. Flores-Arciniega, H. Flores-Zuñiga, J. R. Rangel-Mendez, *Sep. Purif. Technol.*, 2015, **150**, 292.
11 B. C. Pan, J. S. Xu, B. Wu, Z. G. Li, X. T. Liu, *Environ. Sci. Technol.*, 2013, **47**, 9347.
12 L. R. Ramos, J. Ovalle-Turrubiartes, M. A. Sanchez-Castillo, *Carbon*, 1999, **37**, 609.
13 L. Cumbal, A. K. SenGupta, *Environ. Sci. Technol.*, 2005, **39**, 6508.
14 S. Chowdhury, R. Balasubramanian, *Appli. Cata. B: Environ.*, 2014, **160–161**, 307.
15 Y. Q. Chen, Q. K. Zhang, L.B. Chen, H. Bai L. Li, *J. Mater. Chem. A*, 2013, **1**, 13101.
16 M. Barathi, A. S. K. Kumar, C. U. Kumar, N. Rajesh, *RSC Adv.*, 2014, **4**, 53711.
17 S. G. Wang, Y. Ma, Y. J. Shi, W. X. Gong, *J. Chem. Technol. Biotechnol.*, 2009, **84**, 1043.
18 H. X. Wu, T. J. Wang, L. Chen, Y. Jin, Y. Zhang, X. M. Dou, *Ind. Eng. Chem. Res.,* 2009, **48**, 4530.
19 V. Sternitzke, R. Kaegi, J. N. Audinot, E. Lewin, J. G. Hering, C. Annette Johnson, *Environ. Sci. Technol.,* 2012, **46**, 802.
20 M. F. Hochella, A. F. White, *Miner. Soc. Am.,* 1990, **23**, 177.
21 T. Hiemstra, W. H. V. Riemsdijk, *J. Colloi. Interf. Sci.,* 2000, **225**, 94.
22 L. Batistella, L. D. Venquiaruto, M. D. Luccio, J. Vladimir Oliveira, S. B. C. Pergher, M. A. Mazutti, D. Oliveira, A. J. Mossi, H. Treichel, R. Dallago, *Ind. Eng. Chem. Res.,* 2011, **50**, 6871.
23 Jr. W. S. Hummers, R. E. Offeman, *J. Am. Chem. Soc.,* 1958, **80**, 1339.
24 J. Dousma, T. J. Van den Hoven, P. L. De Bruyn, *Inorg. Nucl. Chem.,* 1978, **40**, 1089.
25 J. Dousma, D. den Ottelander, P. L. de Bruyn, *Inorg. Nucl. Chem.,* 1979, **41**, 1565.
26 D. J. Burleson, R.L. Penn, *Langmuir,* 2006, **22**, 402.
27 T. A. Vu, M. M. Reagan, D. S. Li, B. Legg, J. J. De Yoreo, J. F. Banfield, H. Z. Zhang, *Cryst. Eng. Comm.,* 2014, **16**, 1466.
28 R. Chitrakar, S. Tezuka, A. Sonoda, K. Sakane, K. Ooi, T. Hirotsu, *J. Colloid. Interf. Sci.,* 2006, **298**, 602.
29 Y. Tang, X. Guan, J. Wang, N. Gao, R. M. Martin, C. C. Charles, *J. Hazard. Mater.,* 2009, **171**, 774.
30 M. Mohapatra, K. Rout, P. Singh, S. Anand, S. Layek, H. C. Verma, B. K. Mishraa, *J. Hazard. Mater.,* 2011, **186**, 1751.
31 M. Sarkar, P. Acharya, B. Bhattacharya, *J. Colloid Interface Sci.*, 2003, **266**, 28.
32 D. L. Sparks, *Academic Press,* Inc., New York, 1989.
33 S. M. Maliyekkal, A. K. Sharma, L. Philip, *Water Res.,* 2006, **40**, 3497.
34 N. A. Medellin-Castillo, R. Leyva-Ramos, R. Ocampo-Perez, R. F. Garcia de la Cruz, A. Aragon-Pina, J. M. Martinez-Rosales, R. M. Guerrero-Coronado, L. Fuentes-Rubio, *Ind. Eng. Chem. Res.,* 2007, **46**, 9205.
35 Y. H. Li, Q. J. Du, J. J. Wang, T. H. Liu, J. K. Sun, Y. H. Wang, Z. H. Wang, Y. Z. Xia, L. H. Xia, *J. Fluorine Chem.,* 2013, **148**, 67.
36 R. H. Masue, T. A. Loeppert, T.A. Kramer, *Environ. Sci. Technol.,* 2007, **41**, 837.
37 V. K. Saxena, S. Ahmed, *Environ. Geol.,* 2001, **40**, 1084.
38 A. Eskandarpour, M. S. Onyango, A. Ochieng, S. Asai, *J. Hazard. Mater.,* 2008, **152**, 571.
39 M. Kunaschk, V. Schmalz, N. Dietrich, T. Dittmar, E. Worch, *Water Res.,* 2015, **71**, 219.
40 L. Gordon, M. L. Salutsky, H. H. Willard, *Wiley*, New York, 1959.
41 J. M. Bigham, U. Schwertmann, L. Carlson, E. Murad, *Geochim. Cosmochim. Acta*, 1990, **54**, 2743.

